

Various complexity measures in confined hydrogen atom

Sangita Majumdar, Neetik Mukherjee, and Amlan K. Roy*

Department of Chemical Sciences

Indian Institute of Science Education and Research (IISER) Kolkata,

Mohanpur-741246, Nadia, WB, India

Abstract

Several well-known statistical measures similar to *LMC* and *Fisher-Shannon* complexity have been computed for confined hydrogen atom in both position (r) and momentum (p) spaces. Further, a more generalized form of these quantities with Rényi entropy (R) is explored here. The role of scaling parameter in the exponential part is also pursued. R is evaluated taking order of entropic moments α, β as $(\frac{2}{3}, 3)$ in r and p spaces. Detailed systematic results of these measures with respect to variation of confinement radius r_c is presented for low-lying states such as, $1s-3d$, $4f$ and $5g$. For *nodal* states, such as $2s$, $3s$ and $3p$, as r_c progresses there appears a maximum followed by a minimum in r space, having certain values of the scaling parameter. However, the corresponding p -space results lack such distinct patterns. This study reveals many other interesting features.

PACS: 03.65-w, 03.65Ca, 03.65Ta, 03.65.Ge, 03.67-a.

Keywords: *LMC* complexity, *FS* complexity, Confined hydrogen atom.

*Corresponding author. Email: akroy@iiserkol.ac.in, akroy6k@gmail.com.

I. INTRODUCTION

Quantum particles experience intense changes in their physical and chemical properties under spatial confinement. Spherically confined quantum systems have been explored extensively [1], with wide-spread applications in quantum dot, quantum wells and quantum wires, etc. Dramatic changes in various observable properties such as energy spectrum, transition frequencies, transition probabilities, polarizability, chemical reactivity, ionization potential etc., were reported to occur under such situations [1, 2].

Recently there has been a growing interest in using statistical quantities namely, Fisher information (I), Onicescu energy (E), Shannon entropy (S) and Rényi entropy (R) as descriptors of certain chemical, physical properties of a quantum system. Along these lines, *complexity*, another relevant concept, is directly related to aforementioned measures, representing their combined effect. A universal characterization has not been possible, but can be proposed as an indicator of pattern, structure or correlation associated with the distribution function in a given system. It depends on the scale of observation, and constitutes an important area of research with contemporary interest in disordered systems, spatial patterns, language, multi-electronic systems, molecular or DNA analysis, social science, [3–6] etc.

An atom is a complex system; restricting its motion in an enclosure makes it even more fascinating according to a complex world [7, 8]. Complexity, in a system, arises due to breakdown of certain symmetry rules. For finite complexity, the system is either in a state having some less than maximal *order* or not in equilibrium. Stated differently, it vanishes at two limiting cases, *viz.*, when it is (a) at equilibrium (maximum disorder) or b) completely ordered (maximum distance from equilibrium) [8, 9]. It gives a qualitative idea of organization in a system and is considered as a general indicator of structure and correlation. In literature various definitions are available; some of them are Shiner, Davidson, Landsberg (*SDL*) [10–12], López-Ruiz, Mancini, Calbet (LMC) *shape* (C_{LMC}) [13–16], *Fisher-Shannon* (C_{IS}) [17, 18], *Cramér-Rao* [18–20] or *Generalized Rényi-like* complexity [21–23], etc.

The statistical measure of complexity, in product form, can be written as,

$$C_{LMC} = H.D \tag{1}$$

where H represents the information content and D gives an idea of concentration of spatial distribution. In order to satisfy conditions such as reaching minimal values for both extremely ordered and disordered limits, invariance under scaling, translation and replication,

this quantity was criticized [24] and modified [25], giving rise to the expression,

$$C_{LMC} = D.e^S. \quad (2)$$

Principally this gives an interplay between information stored in a system, and measure of a probabilistic hierarchy amongst its observed parts. It has application in diverse fields like detection of periodic, quasi-periodic, linear stochastic, chaotic dynamics [13, 26, 27].

In information theory E signifies a measure of order, because it becomes minimum at equilibrium. Whereas, information entropies like S, R , being maximum at equilibrium, signify disorder. Complexity identifies the extent of balance between order and disorder. Sometimes, I is used in place of E . So far S has been extensively used as disorder parameter. C_{IS} is another measure, obtained by replacing the pre-exponential global factor in C_{LMC} by a local factor like I . It combines global and local characters while preserving desirable properties of complexity. Usefulness of C_{IS} can be judged by looking at the numerous works done for both *free* and *confined* atomic systems, like atomic shell structure, ionization process [17, 18, 20, 28] etc. A more generalized version was also proposed that uses R in place of S , in C_{LMC} and C_{IS} [29]. Later, a scaling factor (b) was introduced in exponential part.

About a decade ago, C_{LMC} was used in the context of Rydberg states of *free* hydrogen atom (FHA) in r, p spaces [30]. Later, C_{LMC} and SDL complexity was employed in atoms [8]. However, in a *confined* hydrogen atom (CHA) complexity measures have been pursued rather rarely. Two major works in this direction involved calculation of C_{IS} in composite space for ground state of CHA under soft and hard confinement [31, 32]. In this endeavor, our focus is to explore four different types of complexity arising out of two order (I, E) and two disorder (S, R) parameters, in both space as functions of confinement radius (r_c). As in the literature [8], we also adopt two b values ($\frac{2}{3}$ for C_{IS} , 1 for C_{LMC}). All calculations were done using the *exact* wave functions of CHA in r space. The p -space wave function is obtained from numerical Fourier transform of r -space counterpart. In the end, pilot calculation are done for eight low-lying states *viz.*, $1s-3d, 4f, 5g$. Organization of this article is as follows. Section II gives a brief account of the theoretical method used; Sec. III presents a detailed discussion on our results, while we conclude with a few remarks in Sec. IV.

II. METHODOLOGY

Exact radial wave function for a CHA can be expressed as [33],

$$\psi_{n,l}(r) = N_{n,l} \left(2r \sqrt{-2\mathcal{E}_{n,l}} \right)^l {}_1F_1 \left[\left[l + 1 - \frac{1}{\sqrt{-2\mathcal{E}_{n,l}}} \right], (2l + 2), 2r \sqrt{-2\mathcal{E}_{n,l}} \right] e^{-r \sqrt{-2\mathcal{E}_{n,l}}}. \quad (3)$$

Here, $N_{n,l}$ denotes normalization constant and $\mathcal{E}_{n,l}$ corresponds to energy of a given state characterized by radial and angular quantum numbers n, l respectively, whereas ${}_1F_1 [a, b, r]$ represents confluent hypergeometric function. Allowed energies are obtained by imposing the boundary condition $\psi_{n,l}(0) = \psi_{n,l}(r_c) = 0$. In this work, generalized pseudospectral (GPS) method was employed to estimate $\mathcal{E}_{n,l}$ of these states. This method has provided very accurate results for various model and real systems including atoms, molecules, some of which could be found in the references [34–36].

The p -space wave function is obtained from Fourier transform of r -space counterpart,

$$\begin{aligned} \psi_{n,l}(p) &= \frac{1}{(2\pi)^{\frac{3}{2}}} \int_0^\infty \int_0^\pi \int_0^{2\pi} \psi_{n,l}(r) \Theta(\theta) \Phi(\phi) e^{ipr \cos \theta} r^2 \sin \theta \, dr d\theta d\phi \\ &= \frac{1}{2\pi} \sqrt{\frac{2l+1}{2}} \int_0^\infty \int_0^\pi \psi_{n,l}(r) P_l^0(\cos \theta) e^{ipr \cos \theta} r^2 \sin \theta \, dr d\theta. \end{aligned} \quad (4)$$

Here $\psi(p)$ is not normalized and needs to be normalized. Integrating over θ and ϕ yields,

$$\psi_{n,l}(p) = (-i)^l \int_0^\infty \frac{\psi_{n,l}(r)}{p} f(r, p) dr. \quad (5)$$

Depending on l , this can be rewritten in following simplified form (m starts with 0),

$$\begin{aligned} f(r, p) &= \sum_{k=2m+1}^{m < \frac{l}{2}} a_k \frac{\cos pr}{p^k r^{k-1}} + \sum_{j=2m}^{m = \frac{l}{2}} b_j \frac{\sin pr}{p^j r^{j-1}}, \quad \text{for even } l, \\ f(r, p) &= \sum_{k=2m}^{m = \frac{l-1}{2}} a_k \frac{\cos pr}{p^k r^{k-1}} + \sum_{j=2m+1}^{m = \frac{l-1}{2}} b_j \frac{\sin pr}{p^j r^{j-1}}, \quad \text{for odd } l. \end{aligned} \quad (6)$$

The values of coefficients a_k, b_j of even- l and odd- l states can easily be computed from Eq. (2). Normalized position and momentum electron densities are expressed as,

$$\rho(\mathbf{r}) = |\psi_{n,l,m}(\mathbf{r})|^2, \quad \Pi(\mathbf{p}) = |\psi_{n,l,m}(\mathbf{p})|^2. \quad (7)$$

Without any loss of generality, let us define complexity in following general form $C = Ae^{b.B}$. The order (A) and disorder parameters (B) may include (E, I) and (R, S)

respectively. With this in mind, we are interested in the following four quantities,

$$C_{ER} = Ee^{bR}, \quad C_{IR} = Ie^{bR}, \quad C_{ES} = Ee^{bS}, \quad C_{IS} = Ie^{bS}. \quad (8)$$

Shannon entropies of a continuous density distribution are written as ('t' stands for *total*),

$$S_{\mathbf{r}} = - \int_{\mathcal{R}^3} \rho(\mathbf{r}) \ln[\rho(\mathbf{r})] d\mathbf{r}; \quad S_{\mathbf{p}} = - \int_{\mathcal{R}^3} \Pi(\mathbf{p}) \ln[\Pi(\mathbf{p})] d\mathbf{p}; \quad S_t = S_{\mathbf{r}} + S_{\mathbf{p}}. \quad (9)$$

Similarly, Rényi entropies of order $\alpha (\neq 1)$ are obtained by taking logarithm of α and β -order entropic moments in respective spaces,

$$R_{\mathbf{r}}^\alpha = \frac{1}{1-\alpha} \ln \left(\int_{\mathcal{R}^3} \rho^\alpha(\mathbf{r}) d\mathbf{r} \right); \quad R_{\mathbf{p}}^\beta = \frac{1}{1-\beta} \ln \left[\int_{\mathcal{R}^3} \Pi^\beta(\mathbf{p}) d\mathbf{p} \right]; \quad R_t = R_{\mathbf{r}}^\alpha + R_{\mathbf{p}}^\beta. \quad (10)$$

The general form of $I_{\mathbf{r}}$, $I_{\mathbf{p}}$ for a particle in a central potential may be simplified as [37],

$$I_{\mathbf{r}} = 4\langle p^2 \rangle - 2(2l+1)|m|\langle r^{-2} \rangle; \quad I_{\mathbf{p}} = 4\langle r^2 \rangle - 2(2l+1)|m|\langle p^{-2} \rangle; \quad I_t = I_{\mathbf{r}}I_{\mathbf{p}}. \quad (11)$$

Finally, E is given by the following expressions in conjugate space,

$$E_{\mathbf{r}} = \int_{\mathcal{R}^3} \rho^2(\mathbf{r}) d\mathbf{r}; \quad E_{\mathbf{p}} = \int_{\mathcal{R}^3} \Pi^2(\mathbf{p}) d\mathbf{p}; \quad E_t = E_{\mathbf{r}}E_{\mathbf{p}}. \quad (12)$$

III. RESULT AND DISCUSSION

At first let us clear a few things before we begin our discussion. All the tables and figures that follow quote the *net* information measures in conjugate r and p space of CHA, which may be partitioned in to radial and angular contributions. In a given space, all results correspond to *net* measures including the *angular* parts. By squeezing the radial boundary of FHA from infinity to a finite region, one progresses to a CHA. As this does not alter the *angular* boundary conditions, angular portion of the information measures in FHA and CHA remains unchanged in both spaces. Further as we are solely interested in *radial* confinement, same will also not change as one modifies r_c values from one to another. However, there will be non-vanishing contribution from l, m quantum numbers. Throughout our calculation, magnetic quantum number m is set to 0. All the aforementioned measures of Eq. (8) have been investigated with respect to r_c , for two selected values of b ($1, \frac{2}{3}$); these are the ones which are widely used in literature. Note that, for $b = 1$, $C_{ES}^{(2)}$ reduces to C_{LMC} ; similarly $C_{IS}^{(1)}$ corresponding to $b = \frac{2}{3}$ refers to C_{IS} of literature. In order to facilitate the discussion, a

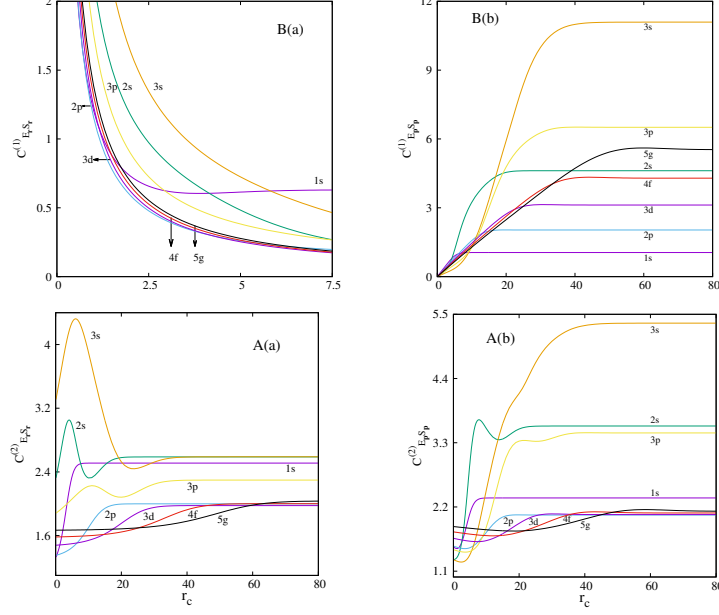


FIG. 1: Variation of $C_{E_r S_r}^{(2)}$, $C_{E_p S_p}^{(2)}$ (bottom row A) and $C_{E_r S_r}^{(1)}$, $C_{E_p S_p}^{(1)}$ (top row B) in CHA with r_c for $1s$ - $3d$, $4f$ and $5g$ states. See text for details.

few words may be devoted to the notation followed. A uniform symbol $C_{order_s, disorder_s}^b$ is used; where the two subscripts refer to two order (E, I) and disorder (S, R) parameters. Another subscript s is used to specify the space; *viz.*, r, p or t (total). Two scaling parameters $b = \frac{2}{3}, 1$ are identified with superscripts 1, 2. These measures are offered systematically for $1s$ - $3d$ as well as $4f$ and $5g$ states in conjugate spaces, with r_c varying in the range of 0.1-100 a.u.

At first, in Fig. 1 $C_{E_r S_r}^{(2)}$, $C_{E_p S_p}^{(2)}$ are plotted against r_c in two bottom panels A(a) and A(b); two similar plots for $C_{E_r S_r}^{(1)}$, $C_{E_p S_p}^{(1)}$ in top two segments B(a) and B(b). Note that the range of r_c is same for all four panels except B(a). Panel A(a) clearly reveals that, $C_{E_r S_r}^{(2)}$ for circular states ($1s$, $2p$, $3d$, $4f$, $5g$) gradually increases with rise of r_c before reaching a threshold corresponding to the FHA result. The particular r_c at which this limiting value is reached tends to grow as l goes up. On the other hand, the same for nodal states ($2s$, $3s$, $3p$) shows a maximum followed by a minimum with r_c and finally converges to respective FHA value. Appearance of such extrema in $C_{E_r S_r}^{(2)}$ thus can be considered as an indication of presence of nodes. Importantly, however, an increase in number of nodes in wave function apparently does not affect the number of extrema produced in $C_{E_r S_r}^{(2)}$. In strong confinement region ($r_c \lesssim 0.4$), for a particular r_c , $C_{E_r S_r}^{(2)}$ enhances with n for the circular states. But in the higher r_c region, significant crossing occurs amongst these states; so this ordering is

TABLE I: $C_{E_r S_r}^{(2)}$, $C_{E_p S_p}^{(2)}$ and $C_{E_t S_t}^{(2)}$ for $1s$, $2s$, $2p$, $3d$ states in CHA at various r_c .

r_c	$C_{E_r S_r}^{(2)}$	$C_{E_p S_p}^{(2)}$	$C_{E_t S_t}^{(2)}$	r_c	$C_{E_r S_r}^{(2)}$	$C_{E_p S_p}^{(2)}$	$C_{E_t S_t}^{(2)}$
$1s$				$2s$			
0.1	1.330123	1.5122	2.0114	0.1	2.325609	1.2984	3.0196
2.0	1.624390	1.5304	2.4860	1.5	2.636436	1.3766	3.6295
3.5	2.012256	1.7709	3.5636	4.1	3.051717	2.3753	7.2489
4.5	2.254326	1.9863	4.4778	6.9	2.624591	3.6385	9.5496
7.5	2.501324	2.3284	5.8242	10.0	2.324233	3.5457	8.2410
10.0	2.510443	2.3533	5.9078	13.0	2.401653	3.3610	8.0721
16.0	2.510692	2.3543	5.9110	38.0	2.588344	3.5864	9.2830
20.0	2.510692	2.3543	5.9110	40.0	2.588344	3.5864	9.2830
$2p$				$3d$			
0.1	1.352613	1.5276	2.0662	0.1	1.479327	1.6617	2.4582
2.5	1.386951	1.4907	2.0676	10.0	1.539579	1.6231	2.4989
5.0	1.449780	1.5013	2.1766	16.0	1.644781	1.7746	2.9189
8.5	1.609479	1.6609	2.6733	20.0	1.753859	1.9185	3.3648
12.0	1.821269	1.8978	3.4565	22.0	1.811337	1.9824	3.5909
14.0	1.912716	1.9966	3.8189	26.0	1.904810	2.0619	3.9276
33.0	1.999251	2.0613	4.1211	56.0	1.977128	2.0698	4.0923
40.0	1.999251	2.0613	4.1211	60.0	1.977128	2.0698	4.0923

no longer maintained. On the other hand, at a fixed low r_c , $C_{E_r S_r}^{(2)}$ for $2s$, $3s$, $3p$ states accelerate with number of nodes. When they have equal number of nodes then the state with lower n has greater complexity. But at weak confinement region this ordering dissolves. Now, from panel A(b) one infers that, for all these reported states there occur a minimum in $C_{E_p S_p}^{(2)}$. Position of this minimum shifts toward right with increase in both n and l . After the minimum point, $C_{E_p S_p}^{(2)}$ for node-less states grows up to reach their terminal value. Whereas for states having nodes ($2s$, $3s$, $3p$), the minimum is preceded by a maximum with increment of r_c . But importantly, these extrema get flattened with progress of n and fall of l for a given n . Now, panel A(c) in Fig. S1 presents variations of the total quantities $C_{E_t S_t}^{(2)}$ for the concerned states. As usual the nodeless states $1s$, $2p$, $3d$, $4f$, $5g$ continually increase with r_c until converging to FHA limit, whereas nodal states go through some extrema before reaching that limit—qualitatively much similar to a pattern encountered in A(a). Next, panels B(a) and B(b) in the top row, delineate that, for all these states $C_{E_r S_r}^{(1)}$ monotonically decline and $C_{E_p S_p}^{(1)}$ enhance with rise of r_c respectively. However, panel B(c) in Fig. S1 shows that, $C_{E_t S_t}^{(1)}$ for circular states elevate with r_c . But, for for the nodal states ($2s$, $3s$, $3p$), there occur some extrema, which thinning out with progress in n, l quantum numbers. From the

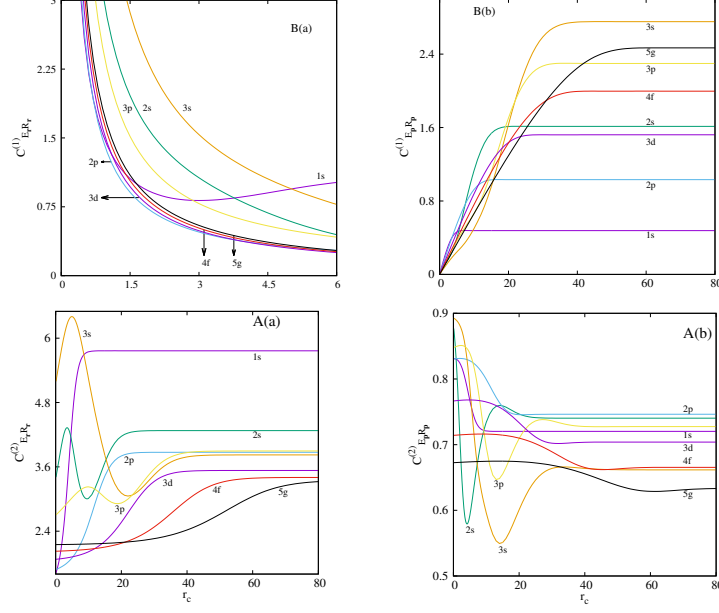


FIG. 2: Changes in $C_{E_r R_r}^{(2)}$, $C_{E_p R_p}^{(2)}$ (bottom row A) and $C_{E_r R_r}^{(1)}$, $C_{E_p R_p}^{(1)}$ (top row B) in CHA with r_c for $1s$ - $3d$, $4f$ and $5g$ states. For more details, see text.

study of these two sets of complexity measures, namely, $C_{ES}^{(2)}$ in A(a)-A(c) and $C_{ES}^{(1)}$ in B(a)-B(c), it is evident that $C_{ES}^{(2)}$ provides better insight about CHA. Hence, we have presented $C_{E_r S_r}^{(2)}$, $C_{E_p S_p}^{(2)}$, $C_{E_t S_t}^{(2)}$ at some selected r_c (not same for all states) in Table I, for $1s$, $2s$, $2p$, $3d$, while the remaining states ($3s$, $3p$, $4f$, $5g$) are offered in Table S1. These results corroborate the conclusions drawn from Figs. 1 and S1. None of these could be directly compared with literature data, as no such works exist, to the best of our knowledge.

Similarly, bottom row of Fig. 2 illustrates the behavior of $C_{E_r R_r}^{(2)}$, $C_{E_p R_p}^{(2)}$ with changes in r_c for the same states of Fig. 1. Panel A(a) shows that, like $C_{E_r S_r}^{(2)}$, here also $C_{E_r R_r}^{(2)}$ for circular states advances to their respective limiting values with growth of r_c . The nodal states ($2s$, $3s$, $3p$) once again display similar pattern as in $C_{E_r S_r}^{(2)}$. At first they cross through a maximum followed by a minimum before eventually coalescing to the respective FHA values. In stronger confinement region, ($r_c \lesssim 0.4$), at a certain r_c , $C_{E_r R_r}^{(2)}$ enhances with n for the circular states. But for higher r_c (FHA limit), there is a decrement in the same for these five states with betterment of n . From panel A(b) it is vivid that, for all these circular states, $C_{E_p R_p}^{(2)}$ diminish with r_c , then attains a shallow minimum and finally stretches to respective FHA value. But for $2s$, $3s$, $3p$ states, prominent minimum pursued by small maximum are observed (before reaching FHA value). Position of these extrema get right

TABLE II: $C_{E_r R_r}^{(2)}$, $C_{E_p R_p}^{(2)}$ and $C_{E_t R_t}^{(2)}$ for $1s$, $2s$, $2p$, $3d$ states in CHA at various r_c .

r_c	$C_{E_r R_r}^{(2)}$	$C_{E_p R_p}^{(2)}$	$C_{E_t R_t}^{(2)}$	r_c	$C_{E_r R_r}^{(2)}$	$C_{E_p R_p}^{(2)}$	$C_{E_t R_t}^{(2)}$
$1s$				$2s$			
0.1	1.62388648	0.83076854	1.34907381	0.1	3.40812187	0.876978	2.988848
1.5	2.00911324	0.82750748	1.66255624	2.0	4.07095921	0.707115	2.878639
3.3	3.06621535	0.80540213	2.46953640	3.5	4.32946637	0.589721	2.553178
4.5	4.06762769	0.77911543	3.16915152	6.5	3.49223860	0.644208	2.249730
6.0	5.08995204	0.74682789	3.80131819	9.6	3.00374145	0.727635	2.185627
18.0	5.76509705	0.72020586	4.15205673	30.0	4.27524770	0.740362	3.165232
25.0	5.76468568	0.72020460	4.15175319	42.0	4.27629214	0.740292	3.165706
30.0	5.76468568	0.72020460	4.15175319	50.0	4.27629299	0.740292	3.165706
$2p$				$3d$			
0.1	1.68688780	0.830403	1.400796	0.1	1.875596	0.766519	1.437680
6.2	2.00463718	0.823814	1.651448	9.5	2.002374	0.765598	1.533015
9.9	2.51770021	0.800244	2.014775	20.0	2.565092	0.733376	1.881177
12.0	2.91667206	0.781037	2.278030	25.0	3.004262	0.711700	2.138136
15.0	3.43010804	0.757407	2.597988	35.0	3.472244	0.702409	2.438936
40.0	3.87153850	0.746249	2.889133	50.0	3.531830	0.703914	2.486106
50.0	3.87153994	0.746249	2.889134	70.0	3.532549	0.703904	2.486576
60.0	3.87153994	0.746249	2.889134	80.0	3.532549	0.703904	2.486576

shifted with n . Moreover, the depth of the minimum enhances with rise of n within a fixed l . The relevant total measures are again displayed in Fig. S2 of supplementary material. For nodeless states, $C_{E_t R_t}^{(2)}$, in panel A(c), like $C_{E_t S_t}^{(2)}$ advances to their FHA value with progression in r_c , while for $2s$, $3s$, $3p$ it passes through a maximum and a minimum before reaching their the same limit. Now panels B(a) and B(b) in top row indicate that, for all these states $C_{E_r R_r}^{(1)}$ gradually decline and $C_{E_p R_p}^{(1)}$ show opposite trend with advances in r_c . However, panel B(c) of Fig. S2 imprints that, $C_{E_t R_t}^{(1)}$ for circular states improves with r_c . But for nodal ($2s$, $2p$, $3s$) states it reaches the FHA threshold by passing consecutive maximum and a minimum. This once again suggests that out of $C_{ER}^{(2)}$ and $C_{ER}^{(1)}$, the former offers more detailed knowledge about CHA, which justifies the quantities produced in Table II, namely, $C_{E_r R_r}^{(2)}$, $C_{E_p R_p}^{(2)}$ and $C_{E_t R_t}^{(2)}$. These are given for four states ($1s$, $2s$, $2p$, $3d$) at eight suitably chosen r_c (not same for all states); Table S2 presents same for $3s$, $3p$, $4f$, $5g$ states. These two Tables II and S2 complement the inferences drawn from Figs. 2 and S2. As in the previous table, here also no literature results could be quoted. Additionally, in r and p spaces $C_{E_r R_r}^{(2)}$ and $C_{E_p R_p}^{(2)}$ exhibit opposite behavior but for $C_{E_r S_r}^{(2)}$ and $C_{E_p S_p}^{(2)}$ an analogous trend is observed. Hence, $C_{E_r R_r}^{(2)}$

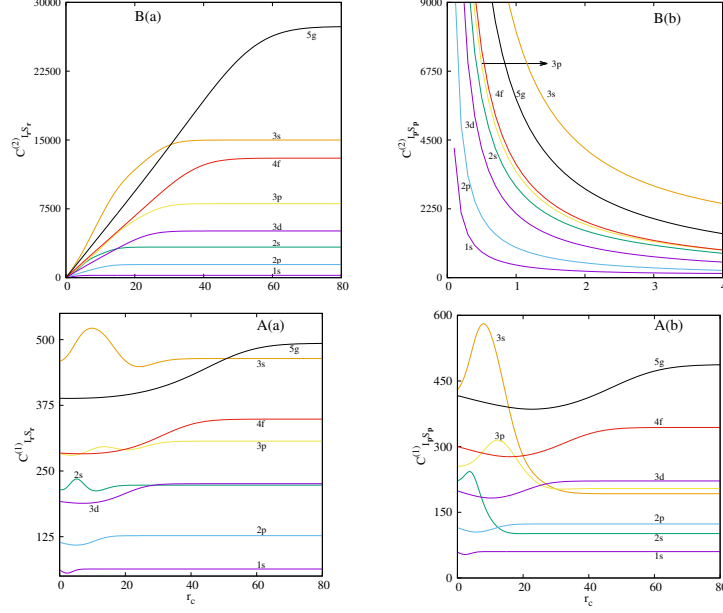


FIG. 3: Variation of $C_{I_r S_r}^{(1)}$, $C_{I_p S_p}^{(1)}$ (bottom row A) $C_{I_r S_r}^{(2)}$, $C_{I_p S_p}^{(2)}$ (top row B) in CHA with r_c for $1s$ - $3d$, $4f$ and $5g$ states. Consult text for more details.

and $C_{E_p R_p}^{(2)}$ turn out to be a relatively better measure of complexity.

Next in Fig. 3 the two rows incorporating panels $\{A(a), A(b)\}$, $\{B(a), B(b)\}$ portray the variation of $\{C_{I_r S_r}^{(1)}, C_{I_p S_p}^{(1)}\}$ and $\{C_{I_r S_r}^{(2)}, C_{I_p S_p}^{(2)}\}$ with changes in r_c . The bottom two panels as well as A(c) of Fig. S3 illustrate that, for circular states, $C_{I_r S_r}^{(1)}$, $C_{I_p S_p}^{(1)}$ and $C_{I_t S_t}^{(1)}$ initially fall with growth of r_c , then attain a minimum and finally converge to respective FHA values. But, for the other three states ($2s$, $3s$, $3p$), $C_{I_r S_r}^{(1)}$ grows to a maximum then falls down to a minimum with advance in r_c and eventually join the FHA result. Whereas, $C_{I_p S_p}^{(1)}$ and $C_{I_t S_t}^{(1)}$, for these three non-circular states only pass through a maximum before reaching their borderline values. On the other hand, top panels B(a) and B(b) portray that, for all eight states considered, $C_{I_r S_r}^{(2)}$ and $C_{I_p S_p}^{(2)}$ consistently progress and reduce respectively with increase in r_c . However, panel B(c) in Fig. S3 shows that, for circular states $C_{I_t S_t}^{(2)}$ enhances with development of r_c and for states with nodes, it passes through a maximum before merging to FHA result. A careful study of Figs. 3 and S3 reveals another interesting feature that, in case of CHA, $C_{I_r S_r}^{(1)}$, $C_{I_p S_p}^{(1)}$, $C_{I_t S_t}^{(1)}$ provides a more detailed account than $C_{I_r S_r}^{(2)}$, $C_{I_p S_p}^{(2)}$, $C_{I_t S_t}^{(2)}$. Thus, to get a quantitative idea, $C_{I_r S_r}^{(1)}$, $C_{I_p S_p}^{(1)}$, $C_{I_t S_t}^{(1)}$ values at some selected r_c 's are given in Tables III ($1s, 2s, 2p, 3d$) and S3 ($3s, 3p, 4f, 5g$). Again no results are available in literature except the lone ground state for $C_{I_S}^{(1)}$ at few r_c values, which are

TABLE III: $C_{I_r S_r}^{(1)}$, $C_{I_p S_p}^{(1)}$ and $C_{I_t S_t}^{(1)}$ for $1s$, $2s$, $2p$, $3d$ states in CHA at selected r_c .

r_c	$C_{I_r S_r}^{(1)}$	$C_{I_p S_p}^{(1)}$	$C_{I_t S_t}^{(1)}$	r_c	$C_{I_r S_r}^{(1)}$	$C_{I_p S_p}^{(1)}$	$C_{I_t S_t}^{(1)}$
$1s^\dagger$				$2s$			
0.1 ^a	61.445391	58.4510	3591.5482	0.1	214.635698	221.5739	47557.6874
1.0 ^b	57.747939	55.7023	3216.6965	0.7	214.216370	224.3204	48053.1193
2.3	55.670758	53.7138	2990.2906	3.0	224.290385	240.5022	53942.3512
4.0	58.707169	55.8278	3277.4955	5.2	234.766329	229.7707	53942.4448
4.7	60.463080	57.2340	3460.5492	11.0	212.022314	126.2148	26760.3588
6.5	62.907313	59.6342	3751.4320	17.0	220.839663	101.9061	22504.9152
30.0 ^c	63.398969	60.3065	3823.3703	43.0	223.025525	101.3888	22612.3074
40.0 ^d	63.398969	60.3065	3823.3703	50.0	223.025525	101.3889	22612.3209
$2p$				$3d$			
0.1	114.078664	114.3281	13042.3998	0.1	191.947614	198.3921	38080.8988
2.5	110.537817	108.7010	12015.5737	3.0	189.827438	192.0738	36460.8929
5.1	108.960438	105.0430	11445.5361	7.2	188.511787	184.6662	34811.7628
7.1	110.071219	105.5415	11617.0842	12.0	191.035748	183.2506	35007.4345
9.5	114.166616	109.1567	12462.0605	17.0	199.745109	190.8078	38112.9401
15.0	124.642286	120.1211	14972.1809	21.0	209.748916	201.1179	42184.2742
34.0	126.882910	123.4402	15662.4635	56.0	225.764533	221.5783	50024.5236
50.0	126.882916	123.4403	15662.4772	70.0	225.764533	221.5783	50024.5236

^aReference result [31]: $C_{I_r S_r}^{(1)} = 61.4476$, $C_{I_p S_p}^{(1)} = 58.9580$, $C_{I_t S_t}^{(1)} = 3622.8276$

^bReference result [31]: $C_{I_r S_r}^{(1)} = 57.7561$, $C_{I_p S_p}^{(1)} = 55.6956$, $C_{I_t S_t}^{(1)} = 3216.7606$

^cReference result [31]: $C_{I_r S_r}^{(1)} = 63.4008$, $C_{I_p S_p}^{(1)} = 60.3087$, $C_{I_t S_t}^{(1)} = 3823.6198$

^dReference result [31]: $C_{I_r S_r}^{(1)} = 63.4008$, $C_{I_p S_p}^{(1)} = 60.3087$, $C_{I_t S_t}^{(1)} = 3823.6198$

[†]Reference values are multiplied with a $8\pi^2 e$ factor in both r and p space.

duly quoted for comparison (for $r_c = 0.1, 1, 30, 40$). Current results are in good agreement with the reported one and may be useful for future references.

Finally, in Fig. 4 the two lower (A(a),A(b)) and upper (B(a)-B(b)) panels depict the alteration of our last complexity measure, *viz.*, $C_{I_r R_r}^{(1)}$, $C_{I_p R_p}^{(1)}$ and $C_{I_r R_r}^{(2)}$, $C_{I_p R_p}^{(2)}$ with variation in r_c . Here, again the bottom row as well as panel A(c) of Fig. S4 shows that, for circular states, $C_{I_r R_r}^{(1)}$, $C_{I_p R_p}^{(1)}$ and $C_{I_t R_t}^{(1)}$ reduce to attain a minimum with rise of r_c and finally assume the fate of FHA. But for three remaining nodal states, $C_{I_r R_r}^{(1)}$ progress via a maximum and minimum successively with growth in r_c ; after that they approach the FHA result. However, $C_{I_p R_p}^{(1)}$ and $C_{I_t R_t}^{(1)}$ for the aforesaid states with nodes, climb a maximum and fall down asymptotically to a constant FHA value. Besides these, panels B(a) and B(b) portray that, for all these reported eight states concerned, $C_{I_r R_r}^{(2)}$ and $C_{I_p R_p}^{(2)}$ rise and fall respectively

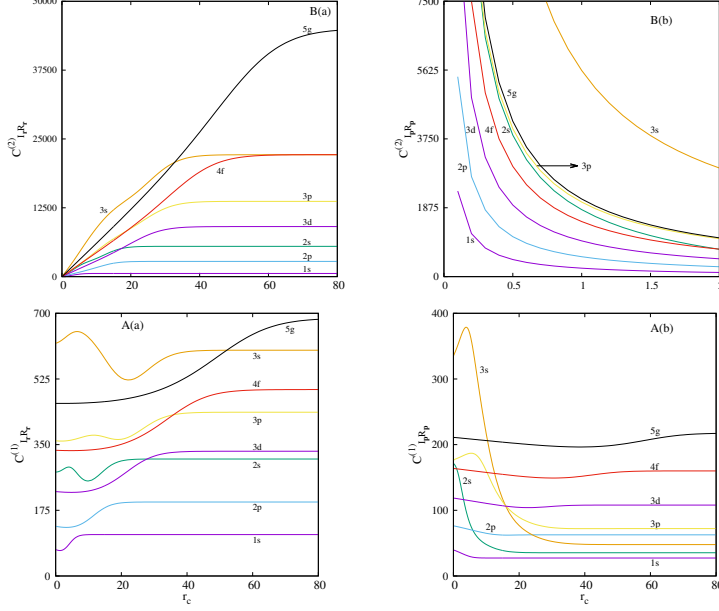


FIG. 4: Plots of $C_{I_R R_R}^{(1)}$, $C_{I_P R_P}^{(1)}$ (bottom row A) and $C_{I_R R_R}^{(2)}$, $C_{I_P R_P}^{(2)}$ (top row B) in CHA with r_c for $1s$ - $3d$, $4f$ and $5g$ states. For further details, see text.

with growth of r_c . However, panel B(c) in Fig. S4 shows that, for circular states $C_{I_t R_t}^{(2)}$ improve with elevation of r_c and for $2s$, $3s$, $3p$ states it proceeds through a maximum before reaching the limiting value at FHA. A closer investigation of Figs. 4 and S4 conveys that, $C_{I_R R_R}^{(1)}$, $C_{I_P R_P}^{(1)}$, $C_{I_t R_t}^{(1)}$ scale the system of this orientation better than $C_{I_R R_R}^{(2)}$, $C_{I_P R_P}^{(2)}$, $C_{I_t R_t}^{(2)}$. Hence, to conclude, the former three measures are offered in Tables IV and S4, at some appropriately chosen r_c . No comparison could be made due to lack of any literature data and hopefully these would be useful in future.

IV. FUTURE AND OUTLOOK

Various complexity measures like C_{ES} , C_{IS} , C_{ER} , C_{IR} are explored for low-lying states of CHA in both r and p space, keeping m fixed at zero. We have pursued our calculation using both global quantity (E) and local quantity (I) as a measure of *order* in a system. Except for some results of C_{IS} in ground state, all these quantities are reported here for the first time. It is found that, $C_{ES}^{(2)}$, $C_{ER}^{(2)}$ offer more detailed explanation than $C_{ES}^{(1)}$, $C_{ER}^{(1)}$ about the system. On the contrary, $C_{IS}^{(1)}$, $C_{IR}^{(1)}$ interpret the behavior of CHA more efficiently than that of $C_{IS}^{(2)}$, $C_{IR}^{(2)}$. Hence, depending upon the nature of complexity measures, it is necessary to determine the appropriate value of b . Accurate results for $C_{ES}^{(2)}$, $C_{ER}^{(2)}$, $C_{IS}^{(1)}$, $C_{IR}^{(2)}$

TABLE IV: $C_{I_r R_r}^{(1)}$, $C_{I_p R_p}^{(1)}$ and $C_{I_t R_t}^{(1)}$ for $1s$, $2s$, $2p$, $3d$ states in CHA at some selected r_c .

r_c	$C_{I_r R_r}^{(1)}$	$C_{I_p R_p}^{(1)}$	$C_{I_t R_t}^{(1)}$	r_c	$C_{I_r R_r}^{(1)}$	$C_{I_p R_p}^{(1)}$	$C_{I_t R_t}^{(1)}$
$1s$				$2s$			
0.1	70.18835424	39.206889	2751.867082	0.1	276.919929	170.569679	47234.143661
1.0	67.97441474	37.745459	2565.725509	2.0	282.717996	143.626221	40605.717425
2.5	70.98469720	34.502985	2449.183973	4.0	290.232344	96.448638	27992.514409
5.0	93.90104729	29.677676	2786.764914	7.0	268.480761	61.038709	16387.719163
5.8	100.48737687	28.715280	2885.523167	9.8	253.236641	48.608701	12309.504305
6.8	105.75702471	27.975405	2958.595632	18.0	300.561968	36.584635	10995.950138
23.0	110.34101779	27.379301	3021.060018	50.0	311.686645	35.411689	11037.350749
30.0	110.34101779	27.379301	3021.060018	70.0	311.686648	35.411668	11037.344253
$2p$				$3d$			
0.1	132.174030	76.150268	10065.087867	0.1	224.853345	118.438787	26631.357655
3.4	129.499950	72.573286	9398.237011	16.0	244.855787	106.300730	26028.349158
5.8	132.007059	69.694271	9200.135775	20.0	266.977357	104.494337	27897.622145
8.2	140.266419	66.892350	9382.750441	23.0	286.056400	104.096971	29777.604868
10.0	150.439765	65.033889	9783.683044	26.0	303.369560	104.554144	31718.544807
13.0	170.727938	62.902501	10739.214335	56.0	332.420701	107.955748	35886.725520
60.0	197.127576	62.701899	12360.273469	86.0	332.423192	107.955697	35886.977628
70.0	197.127576	62.701899	12360.273469	90.0	332.423192	107.955697	35886.977628

(radial *plus* angular) are provided for $1s$ - $3d$, $4f$ and $5g$ states of CHA, most of them for the first time. Further, an investigation of all these quantities in the realm of Rydberg states under different kinds of confined environment, as well as the correlation between complexity and periodicity in many-electron atomic systems may be worthwhile pursuing.

V. ACKNOWLEDGEMENT

Financial support from DST SERB, New Delhi, India (sanction order: EMR/2014/000838) is gratefully acknowledged. SM is obliged to IISER-K for supporting her JRF. NM thanks DST SERB, New Delhi, India, for a National-post-doctoral fellowship (sanction order: PDF/2016/000014/CS).

-
- [1] J. R. Sabin, E. Brändas and S. A. Cruz (Eds.), *The Theory of Confined Quantum Systems*, Parts I and II, *Advances in Quantum Chemistry*, Vols. 57 and 58 (Academic Press, 2009).

- [2] K. D. Sen (Ed.), *Electronic Structure of Quantum Confined Atoms and Molecules*, (Springer, Switzerland, 2014).
- [3] O. A. Rosso, M. T. Martin and A. Plastino, *Physica A* **320**, 497 (2003).
- [4] C. R. Shalizi, K. L. Shalizi and R. Haslinger, *Phys. Rev. Lett.* **93**, 118701 (2004).
- [5] K. Ch. Chatzisavvas, Ch. C. Moustakidis and C. P. Panos, *J. Chem. Phys.* **123**, 174111 (2005).
- [6] P. A. Bouvrie, J. C. Angulo and J. S. Dehesa, *Physica A* **390**, 2215 (2011).
- [7] N. Goldenfeld and L. P. Kadanoff, *Science* **284**, 87 (1999).
- [8] K. D. Sen (Ed.), *Statistical Complexity: Applications in Electronic Structure*, (Springer, 2012).
- [9] K. D. Sen (Ed.), *Reviews of Modern Quantum Chemistry: A Celebration of the Contributions of Robert G. Parr*, Vol. 1 (World Scientific, Singapore, 2002).
- [10] P. T. Landsberg, *Phys. Lett. A* **102**, 171 (1984).
- [11] P. T. Landsberg and J. S. Shiner, *Phys. Lett. A* **245**, 228 (1998).
- [12] J. S. Shiner, M. Davison and P. T. Landsberg, *Phys. Rev. E* **59**, 1459 (1999).
- [13] R. López-Ruiz, H. L. Mancini and X. Calbet, *Phys. Lett. A* **209**, 321 (1995).
- [14] C. Anteneodo and A. R. Plastino, *Phys. Lett. A* **223**, 348 (1996).
- [15] R. G. Catalán, J. Garay and R. López-Ruiz, *Phys. Rev. E* **66**, 011102 (2002).
- [16] J. R. Sánchez and R. López-Ruiz, *Physica A* **355**, 633 (2005).
- [17] K. D. Sen, J. Antolín and J. C. Angulo, *Phys. Rev. A* **76**, 032502 (2007).
- [18] J. C. Angulo, J. Antolín and K. D. Sen, *Phys. Lett. A* **372**, 670 (2008).
- [19] J. S. Dehesa, P. Sánchez-Moreno and R. J. Yáñez, *J. Comput. Appl. Math.* **186**, 523 (2006).
- [20] J. Antolín and J. C. Angulo, *Int. J. Quant. Chem.* **109**, 586 (2009).
- [21] X. Calbet, R. López-Ruiz, *Phys. Rev. E* **63**, 066116 (2001).
- [22] M. T. Martin, A. Plastino and A. O. Rosso, *Physica A* **369**, 439 (2006).
- [23] E. Romera and A. Nagy, *Phys. Lett. A* **372**, 6823 (2009).
- [24] D. P. Feldman and J. P. Crutchfield, *Phys. Lett. A* **238**, 244 (1998).
- [25] R. López-Ruiz, *Biophys. Chem.* **115**, 215 (2005).
- [26] T. Yamano, *J. Math. Phys.* **45**, 1974 (2004).
- [27] T. Yamano, *Physica A* **340**, 131 (2004).
- [28] J. C. Angulo and J. Antolín, *J. Chem. Phys.* **128**, 164109 (2008).
- [29] J. C. Angulo, J. Antolín and R. O. Esquivel, in *Statistical Complexity: Applications in Electronic Structure*, K. D. Sen (Ed.), pp. 167 (Springer, 2012).

- [30] J. Sañudo and R. López-Ruiz, Phys. Lett. A **372**, 5283 (2008).
- [31] N. Aquino, A. Flores-Riveros and J. F. Rivas-Silva, Phys. Lett. A **377**, 2062 (2013).
- [32] Á. Nagy, K. D. Sen and H. E. Montgomery Jr., Phys. Lett. A **373**, 2552 (2009).
- [33] B. L. Burrows and M. Cohen, Int. J. Quant. Chem. **106**, 478 (2006).
- [34] A. K. Roy, J. Phys. G **30**, 269 (2004).
- [35] K. D. Sen and A. K. Roy, Phys. Lett. A **357**, 112 (2006).
- [36] A. K. Roy, Int. J. Quant. Chem. **115**, 937 (2015); *ibid.*, **116**, 953 (2016).
- [37] E. Romera, P. Sánchez-Moreno and J. S. Dehesa, Chem. Phys. Lett. **414**, 468, (2005).

